Speaks *International Journal of Mechanical and Materials Engineering* (2020) 15:2
https://doi.org/10.1186/s40712-019-0113-6

International Journal of Mechanical and Materials Engineering

ORIGINAL PAPER Open Access

Effect of concentration, aging, and annealing on sol gel ZnO and Al-doped ZnO thin films

D. T. Speaks

Abstract

Presented are experimental results on the effect of concentration, aging, and annealing time on the optical and structural properties of sol gel zinc oxide (ZnO) and Al-doped ZnO thin films. ZnO and ZnO:Al thin films were fabricated on glass substrates using spin coating followed by annealing. XRD confirmed that the films are polycrystalline wurtzite. For low concentration films (0.2 and 0.4 M), grain size increased with aging time up to 72 hours. For high concentration samples (0.6 and 0.8 M), grain size increased only up to 48 hours. Additional aging resulted in a decrease in the grain size. The largest grain sizes were found for 0.4 M at 72 hours and 0.6 M at 48 hours. The band gap tended to decrease with increasing aging time for all concentrations. The smallest band gap for each aging time (24, 48, and 72 hours) was observed for 0.6 M films. These results suggest that higher concentration sol gel near 0.6 M may yield better properties with shorter aging times than 0.2 and 0.4 M films. Annealing data suggests that 350 ^{o}C is the minimum annealing at 1 hour to achieve high-quality films and higher concentration ZnO films have stronger diffraction peaks. ZnO:Al also exhibits stronger diffraction peaks and a larger blue shift of the band edge with increasing sol gel concentration.

Keywords: Zinc oxide, sol gel, band gap, optical properties, thin films

Introduction

Transparent conductive oxides (TCOs) have many important applications. Because of their unusual combination of electrical conductivity and optical transparency, they are often used as electrical contacts for light-emitting diodes and solar cells (Rajeh, Khirouni, Amlouk, & Guermazi, 2015). Indium tin oxide (ITO) was one of the first TCOs that was used for contacts for solar cells; however, starting 1980's, zinc oxide (ZnO) started to be extensively researched (Demichelis, Minetti-Mezzetti, Smurro, Tagliagerro, & Tresso, 1985). While ITO and ZnO have many similar properties such as large band gaps (3.37 eV for ZnO and 3.4 eV for ITO) and high electrical conductivities, ZnO has the additional benefit of being nontoxic and less expensive. Since ZnO is a II–VI semiconductor with a direct gap, it has a strong optical absorption near the band edge, and it has a large ~60 meV exciton-binding energy (Janotti & Van de Walle, 2009a; Yan et al., 2016). These properties coupled with ZnO's high chemical stability, high thermal conductivity, and low dielectric constant make ZnO one of the most important TCOs to date.

Much of the current research on zinc oxide has been centered around a few key areas: (1) exploring nanomaterials such as ZnO nanowires (Rabina, Rai, & Swain, 2019), (2) band gap engineering with MgO, CdO, etc. to control the optical properties for devices such as solar cells (Ref (Rabina et al., 2019)), (3) determination of the n-type preference of ZnO and explaining the difficulty in making p-type ZnO(Janotti & Van de Walle, 2009b), and (4) ZnO compatibility with GaN devices (Janardhanam, Jyothi, Lee, Reddy, & Choi, 2019). It has been shown that ZnO is almost always n-type even when doped p-type, and much debate has centered around the mechanism. Some research suggests it is the tendency for ZnO to have oxygen vacancies, which makes films n-type, while other research suggests it is H impurities which act as shallow donors (Janotti & Van de Walle, 2009b; Wang et al., 2012; Zen, Duan, Yang, Xu, & Cai, 2010). What is

Correspondence: derrick.speaks@titantechenergy.com
Titan Tech Energy, Phoenix, Arizona, USA

agreed upon however is the very strong propensity to be n-type. This tendency creates many challenges for device fabrication, especially when a p-type layer is required. In addition to the origins of the conductivity type, recent research has been centered on doping and alloying with other oxides such as MgO and CdO. For example, Yu et al. provide a model for determining the band edge positions and the band gaps for a variety of ZnO-based materials doped with Cd, Be, Mg, Ca, Sr, and Ba (Yu, Zhang, Zhang, Wang, & Wu, 2019). This means that doped ZnO provides an excellent material system to precisely control the optical and electronic materials for many different device applications.

Much of the current research focuses on understanding the mechanisms of defects and doping in ZnO, and often developing a cost-effective method of creating ZnO thin films is not a major concern. Indeed, since many of these applications require precise control of the defects in the films, methods like sol gel are often avoided. However, if the sol gel process could be improved to the point that it could make high-quality, low defect films, it would be more widely used both in research and in industry.

While ZnO, like most TCOs, can be fabricated from a variety of film deposition techniques, including PLD (Mayer et al., 2012), CVD (Terasako, Ochi, Yagi, Nomoto, & Yamamoto, 2018), magnetron sputtering (Goncalves, Barrozo, Brito, Viana, & Cunha, 2018), sol gel (Meng, Zhao, Xu, Wang, & Liu, 2018), and spray pyrolysis (Jayaraman, Alvarez, Bizarro, & Amador, 2018), sol gel is especially interesting because of its low cost and scalability. While low cost, the sol gel process is very complex and includes many different reactions before a final film is made. The sol gel process has many steps which include hydrolysis of the molecular precursor, polymerization, condensation, nucleation, and finally growth. Chu et al. provide the following model to describe the chemistry for ZnO sol gel using zinc acetate (Chu et al., 2012) Fig. 1.

Here R-OH is used to represent a general alcohol, with the OH being the functional group. The zinc precursor concentration will have an impact on the reaction shown in Fig. 1 as will temperature during mixing and aging. Chemicals used for the zinc precursor and the solvent are also important considerations. Common zinc precursors include zinc nitrate and zinc acetate. Zinc nitrate has the drawback that removal of the anionic components can be difficult once the thin films are fabricated. Zinc acetate has the advantage that the acetate group will decompose during annealing. For sol gel applications, the solvent must have a comparatively high dielectric constant in order to dissolve the precursors. Dielectric constant is related to chain length, and for this reason, carbon chain length in the alcohol tends to not exceed 4 (Znaidi, 2010). Methanol (CH_3OH) and 2-propanol ($CH_3CH(OH)CH_3$) are two common solvents. Compared to 2-propanol, methanol has a higher dielectric constant (32.35 vs 18.62) and a higher solubility limit for the precursors; however it has a lower boiling temperature (64.7 vs 82.2 °C)(Znaidi, 2010).

Sol gel reactions have many important parameters. These include solvent, precursors, mixing temperature, concentration (Amari, Mahroug, Boukhari, Deghfel, & Selmi, 2018), pH (El Hamidi et al., 2018; Yaun, Xu, & Huang, 2014), aging time, and aging temperature (Ibrahim, Al-Shomar, & Ahmed, 2013). However, these parameters have not been optimized for many systems, including ZnO. Many recent papers use a molar concentration of the zinc precursor of 0.2 to 0.4 M. Amari et al. recently found that higher molar concentration of Zn precursors leads to an increase in the film quality of ZnO thin films until very high molar concentration is reached (Zen et al., 2010). This was demonstrated by an increase in grain size as a function of increasing Zn molar concentration. In addition, the %T was large, only dropping significantly after concentrations in excess of 0.7 M were used. The results were limited to films that were aged for 24 hours only, so, it is currently not known if the effect of increasing concentration holds with increasing aging time. Here we seek to answer that question by finding the optimal processing conditions for ZnO sol gel that includes both concentration and aging time.

Methods

ZnO thin films were prepared on glass using a sol gel process followed by spin coating. Zinc acetate dihydrate ($Zn(OOCCH_3)_2{*}2H_2O$ Alfa Aesar) was used as the Zn precursor. 2-Propanol was used as the solvent with

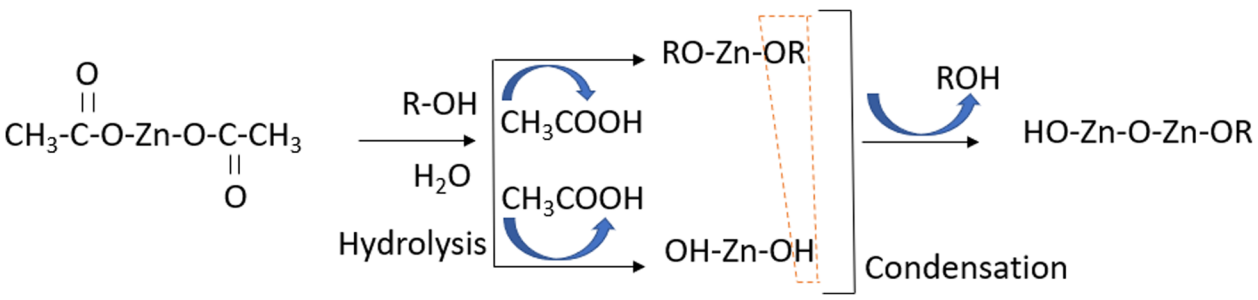

Fig. 1 ZnO sol gel reaction with zinc acetate

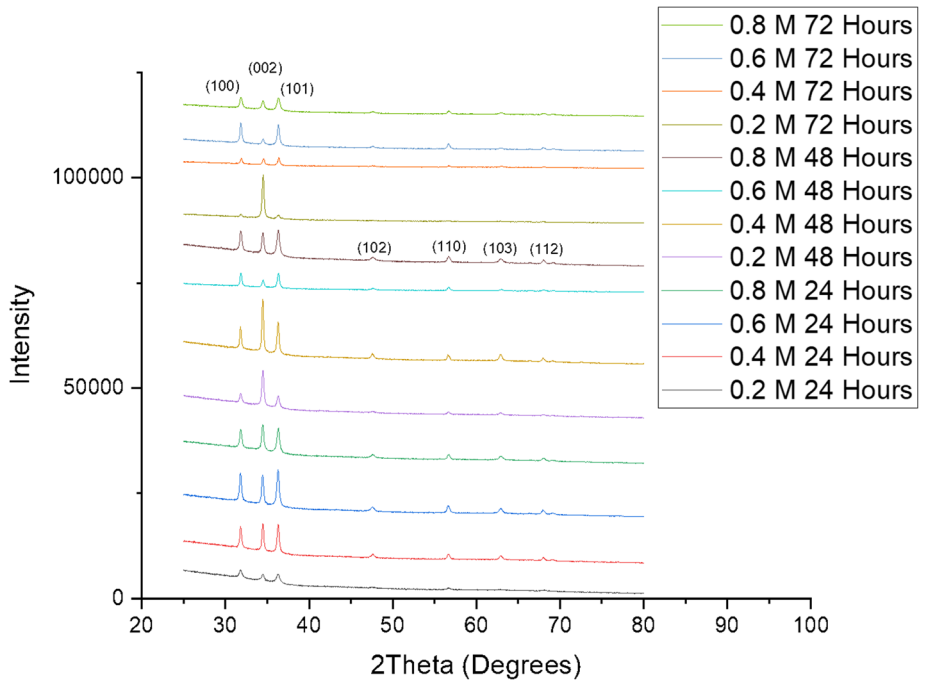

Fig. 2 XRD patterns by concentration and age time

ethanolamine (MEA, $HOCH_2CH_2NH_2$, Alfa Aesar) as the stabilizer. A concentration of 0.2, 0.4, 0.6, or 0.8 mol/L of zinc precursor solutions was prepared with a ratio of 1:1 between the MEA stabilizer and the Zn precursor. The final solutions were fabricated by stirring 15 mL at 50 °C for 30 minutes. The solutions were all aged at room temperature for 24, 48, and 72 hours. Each film layer was deposited using a spin coater operating at 2000 rpm for 30 seconds. After each layer was added, films were placed in a furnace at 250 °C for 20 minutes to promote the rapid evaporation of the

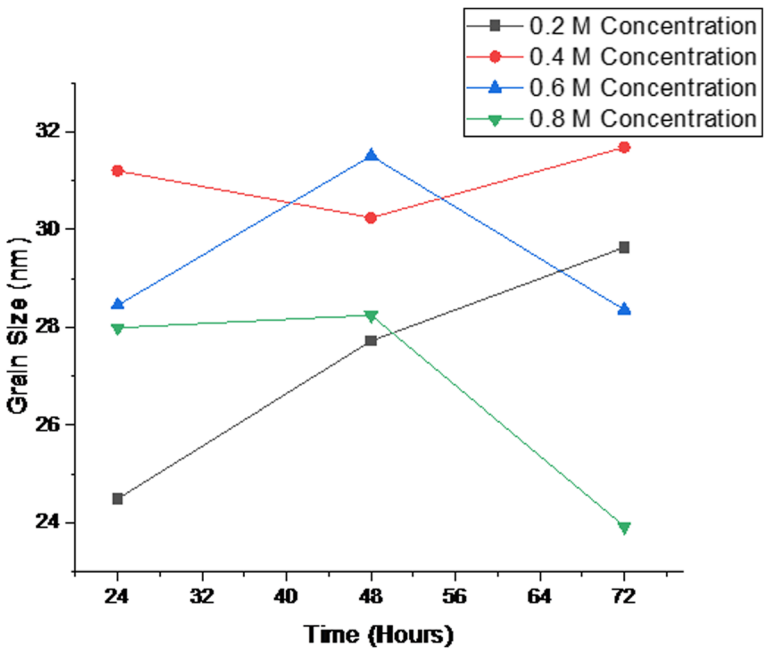

Fig. 3 Grain size as a function of aging time

Table 1 Grain size and lattice constants by concentration and aging time

Concentration (M)	Time (hours)	D (nm)	a (A)	c (A)
0.2	24	24.49179	3.248841	5.194026
0.4	24	31.20438	3.243845	5.198919
0.6	24	28.45677	3.245508	5.201369
0.8	24	27.99077	3.243845	5.198919
0.2	48	27.71949	3.245508	5.198919
0.4	48	30.24057	3.245508	5.198919
0.6	48	31.50806	3.242183	5.194026
0.8	48	28.24857	3.242183	5.196471
0.2	72	29.6393	3.240523	5.194026
0.4	72	31.68332	3.237209	5.189143
0.6	72	28.35989	3.242183	5.196471
0.8	72	23.92255	3.242183	5.194026

solvent and the removal the organic residuals. This process was repeated until eight layers were fabricated for each film. Finally, the films were annealed in a furnace in ambient at 500 °C for 2 hours. Films were analyzed using a Phillips X'PERT MPD XRD system. A Perkins Elmer Lambda 1050 was used to collect optical absorption data. To study the annealing properties, films, using the same method described above, were fabricated and annealed for 1 hour at 150, 250, 350, and 450 °C. Finally, Al-doped ZnO thin films were also fabricated using aluminum chloride hexahydrate ($AlCH_3{}^*6H_2O$) from Alfa Aesar. Doping concentrations of 1.5 and 3.0% Al were used in both low concentration (0.2 M) and high concentration (0.6 M) films.

Results and discussion

X-ray diffraction was used to determine crystal structure, crystal orientation, and crystal size. All films are polycrystalline wurtzite and display multiple diffraction peaks corresponding to multiple crystallographic orientations.

The following figure shows the XRD scans for each film: (Fig. 2).

The Bragg equation was used to compute the interplanar spacing, d:

$$n\lambda = 2\mathrm{d}\ sin\theta \tag{1}$$

where n is the order of the diffraction (typically n = 1), λ is the X-ray wavelength, d is the spacing between atomic planes, and θ is the Bragg angle.

Since zinc oxide is a hexagonal crystal structure, it requires two lattice constants to describe its unit cell, and the following equation is used to relate d to the lattice constants, a and c, and the Miller indices, h,k and l:

$$\frac{1}{d_{nk_l}^2} = \frac{4}{3}\left(\frac{h^2 + hk + k^2}{a^2}\right) + \frac{l^2}{c^2} \tag{2}$$

For all films, the major diffraction peaks occur at low 2Theta and correspond to the <100>, <002>, and < 101> planes. At higher 2θ's, the <102>, <110>, <103>, and < 112> planes are often observed but at a much lower intensity.

Setting n = 1 yields:

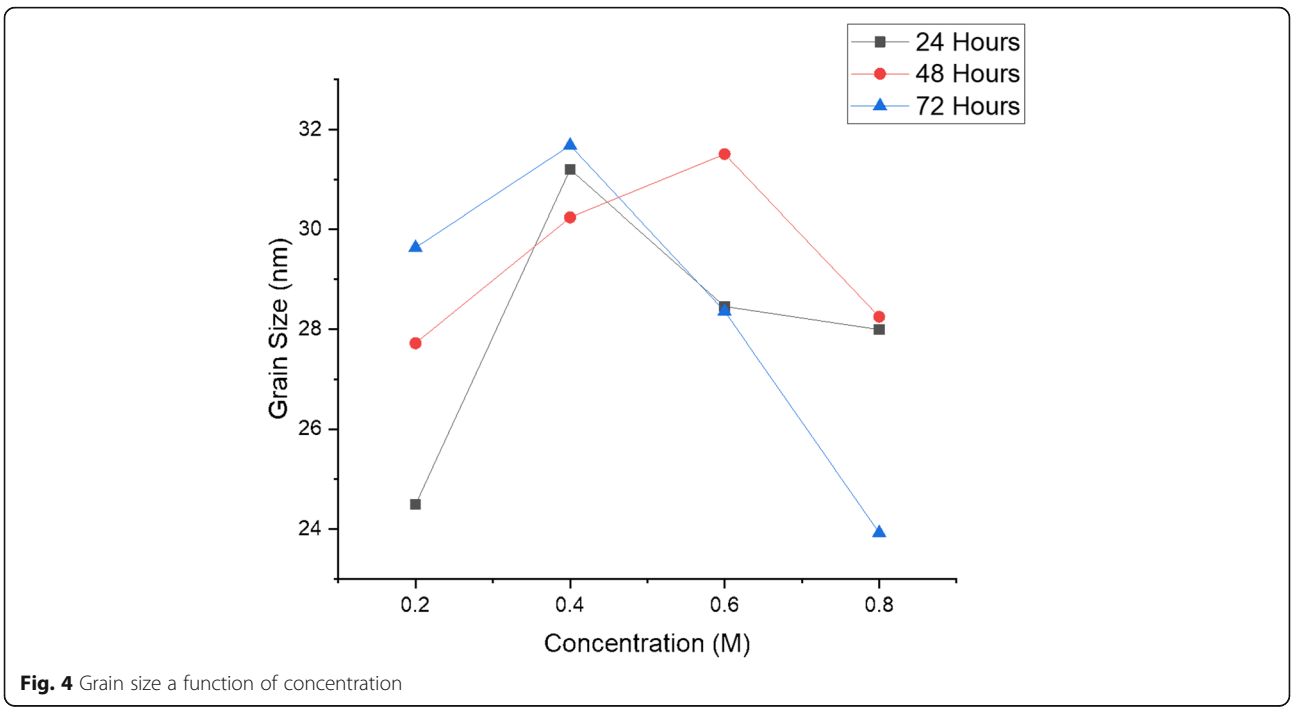

Fig. 4 Grain size a function of concentration

$$sin^2\theta = \frac{\lambda^2}{4a^2} * \left(\frac{4}{3} * \left(\frac{h^2 + hk + k^2}{a^2}\right) + \left(\frac{a}{c}\right)^2 * l^2\right) \quad (3)$$

While any observed lattice plane can be used to solve Eq. 3, a reduced form of the equation can be derived if hkl = <100> is used to solve for a, and hkl = <002> is used to solve for c. The resulting equations are:

$$a = \frac{\lambda}{\sqrt{3}\ sin\theta} \quad (4)$$

$$c = \frac{\lambda}{\sin\theta} \quad (5)$$

The computed *d* spacing is consistent with the JCPDS data for hexagonal wurtzite ZnO (Rajeh et al., 2015). The supplemental section shows the computed *d* spacing, the reference d spacing, the percent deviation of the computed to the reference d spacing, the full width at half maximum (FWHM), and the relative peak intensity normalized to the largest peak. The percent difference between the reference *d* spacing and the actual *d* spacing ranges from 0.003% to 0.4%. This is consistent with values found by Amari et al. that ranged from 0.01% to 0.56%.

The width of the Bragg peaks is influenced by the crystal size, and the Debye-Scherrer equation shows the relationship between peak width and crystal size:

$$D = \frac{0.9\lambda}{B\ \cos\theta} \quad (6)$$

where *D* is the average grain size, λ is the X-ray wavelength, B is the FWHM, and θ is the Bragg angle (Table 1).

The grain size, computed from the Debye-Scherrer equation, can be used to determine the optimal conditions for film processing. Generally, larger grains are more desirable as this results in higher-quality films that necessarily have fewer grain boundaries. The following figure shows the computed grain size as a function of time for each concentration (Fig. 3).

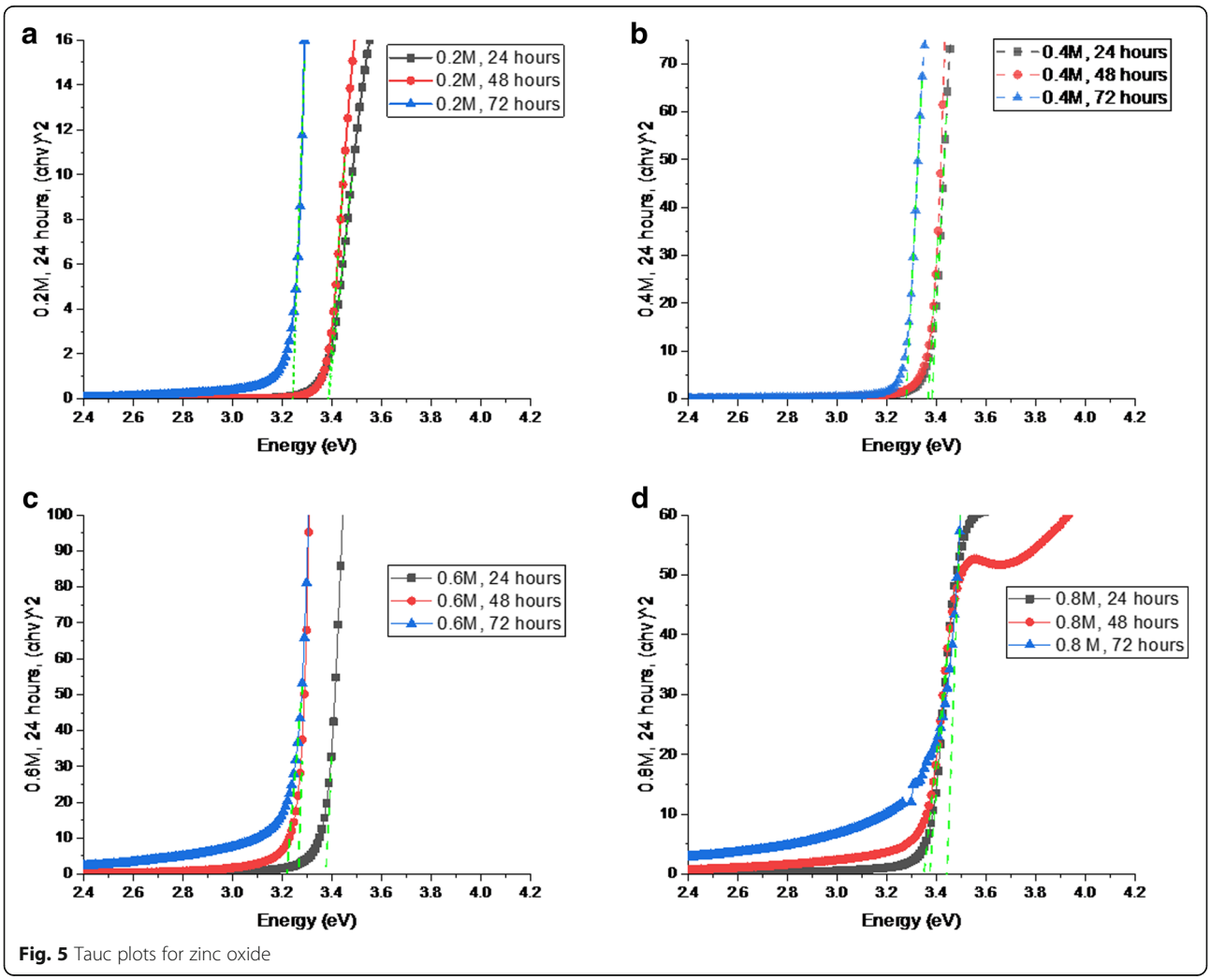

Fig. 5 Tauc plots for zinc oxide

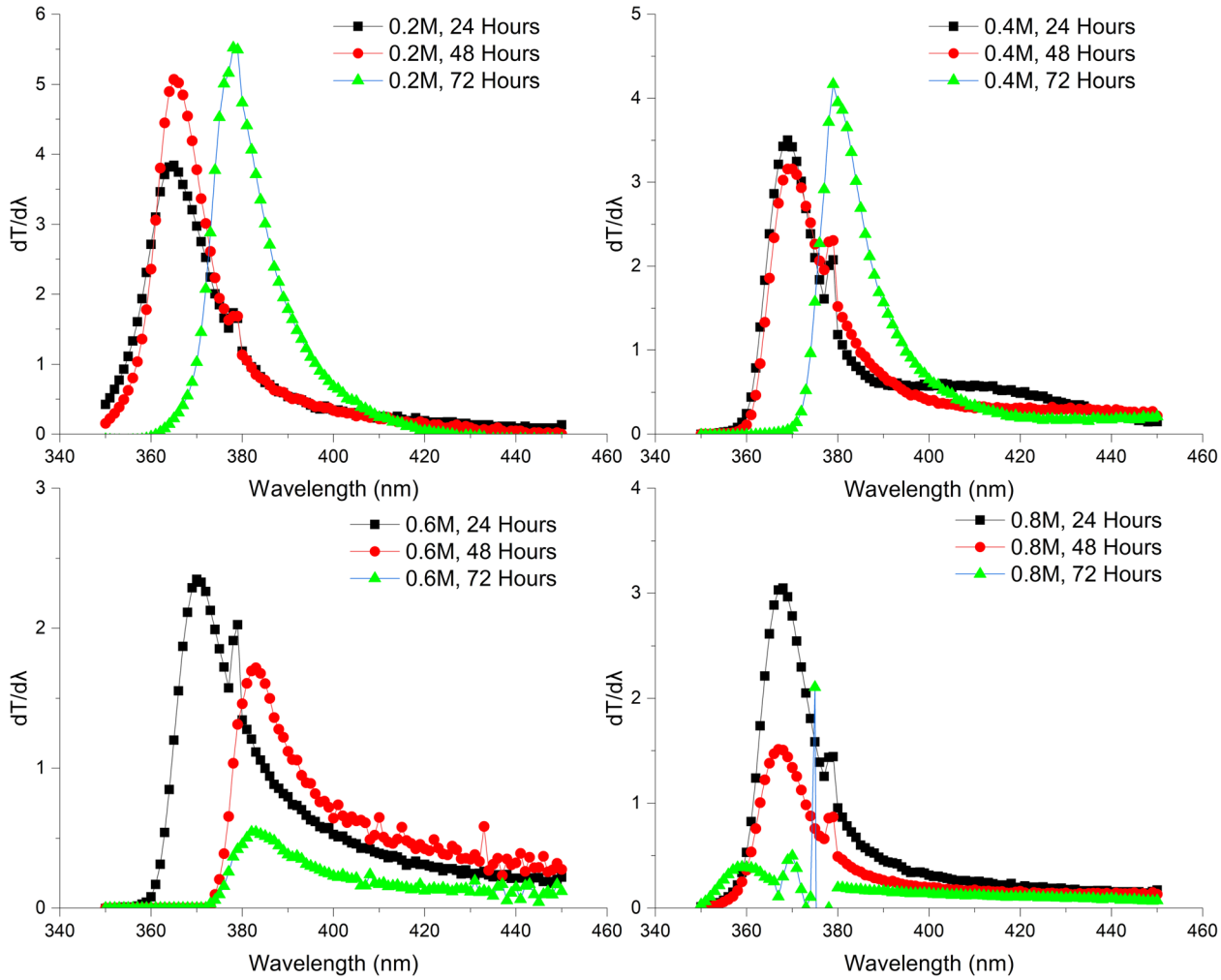

Fig. 6 dT/dλ plots for ZnO

Table 2 Band gap

Concentration (Mol)	Age time (hours)	Band gap (eV) dT/dλ method	Band gap (eV) Tauc method	R^2	Δ (eV)
0.2	24	3.40	3.36	0.995772	0.04
0.2	48	3.40	3.38	0.995986	0.02
0.2	72	3.28	3.27	0.998545	0.01
0.4	24	3.36	3.38	0.997285	0.02
0.4	48	3.36	3.27	0.992703	0.02
0.4	72	3.27	3.28	0.998453	0.01
0.6	24	3.35	3.38	0.999094	0.03
0.6	48	3.29	3.38	0.997849	0.09
0.6	72	3.24	--	--	--
0.8	24	3.37	3.37	0.997265	0.00
0.8	48	3.35	3.35	0.99553	0.00
0.8	72	3.45	--	--	--

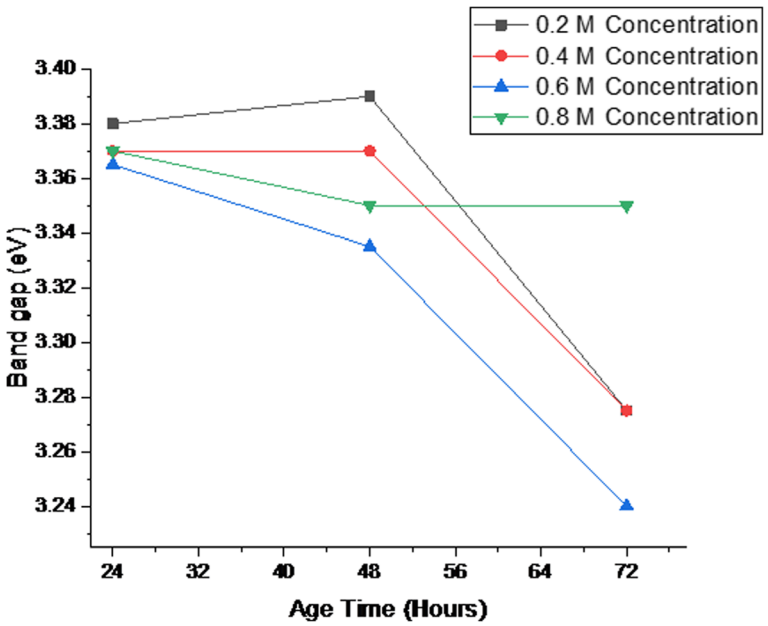

Fig. 7 Band gap as a function of time

As the time increases for 0.2 and 0.4 M samples, the grain size tends to increase. This suggests that lower concentration samples display increasing film quality as the aging time increases. For both the 0.6 and 0.8 M samples, the grain size initially increases with aging time but sharply decreases after 48 hours. This suggests that extending aging beyond 48 hours decreases film quality for higher concentration samples. The result is that higher concentration samples will age more quickly and achieve peak grain size sooner than lower concentration samples.

Another important consideration for the film growth conditions that lead to the largest grain size is the influence of concentration for a fixed aging time. Figure 4 shows the

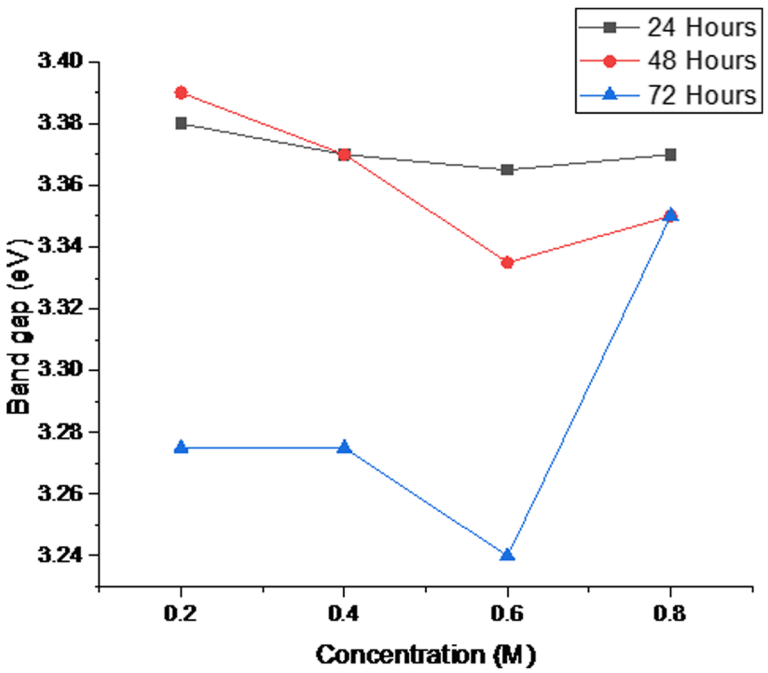

Fig. 8 Band gap as a function of concentration by aging time

grain size as a function of concentration for each aging time.

In all cases, the 0.4 or the 0.6 M samples had the largest grain size. Surprisingly, the largest grain sizes were not found in the lower 0.2 samples exclusively, which are the typical concentrations used, but rather in the moderate and high concentration samples of 0.4 and 0.6 M. In addition, the maximum grain size for 0.6 M (31.5 nm) was achieved after just 48 hours of aging, rather than the 72 hours necessary for the 0.4 M sample (31.7 nm).

The optical properties of ZnO can be divided into two distinct regions: (1) a high energy region UV region and (2) a lower energy visible and near IR region. The UV region contains band gap information. The visible region overlaps with the largest peaks in the solar radiation spectrum (Gueymard, Myers, & Emery, 2002), so it contains wavelengths that are often targeted for absorption in solar cells. Thus, it is important for a TCO to be transparent in this region. In the next section, both regions are investigated to determine the band gap, band tailing, and percent transmittance (%T).

The optical band gaps were estimated using the Tauc equation (Tan et al., 2005; Tauc, Grigorovici, & Vancu, 1966; Uzar, 2018; Wannes & Zaghousani, 2018)

$$(\alpha h\nu)^n = A\left(h\nu - E_g\right) \tag{7}$$

where α is the absorption coefficient, $h\nu$ is the photon energy, A is a constant, n denotes the type of transition (for direct gap transitions n = 2), and E_g is the band gap (Wannes & Zaghousani, 2018). Extrapolation of the linear region of the curve of $(\alpha h\nu)^2$ to zero yields the band

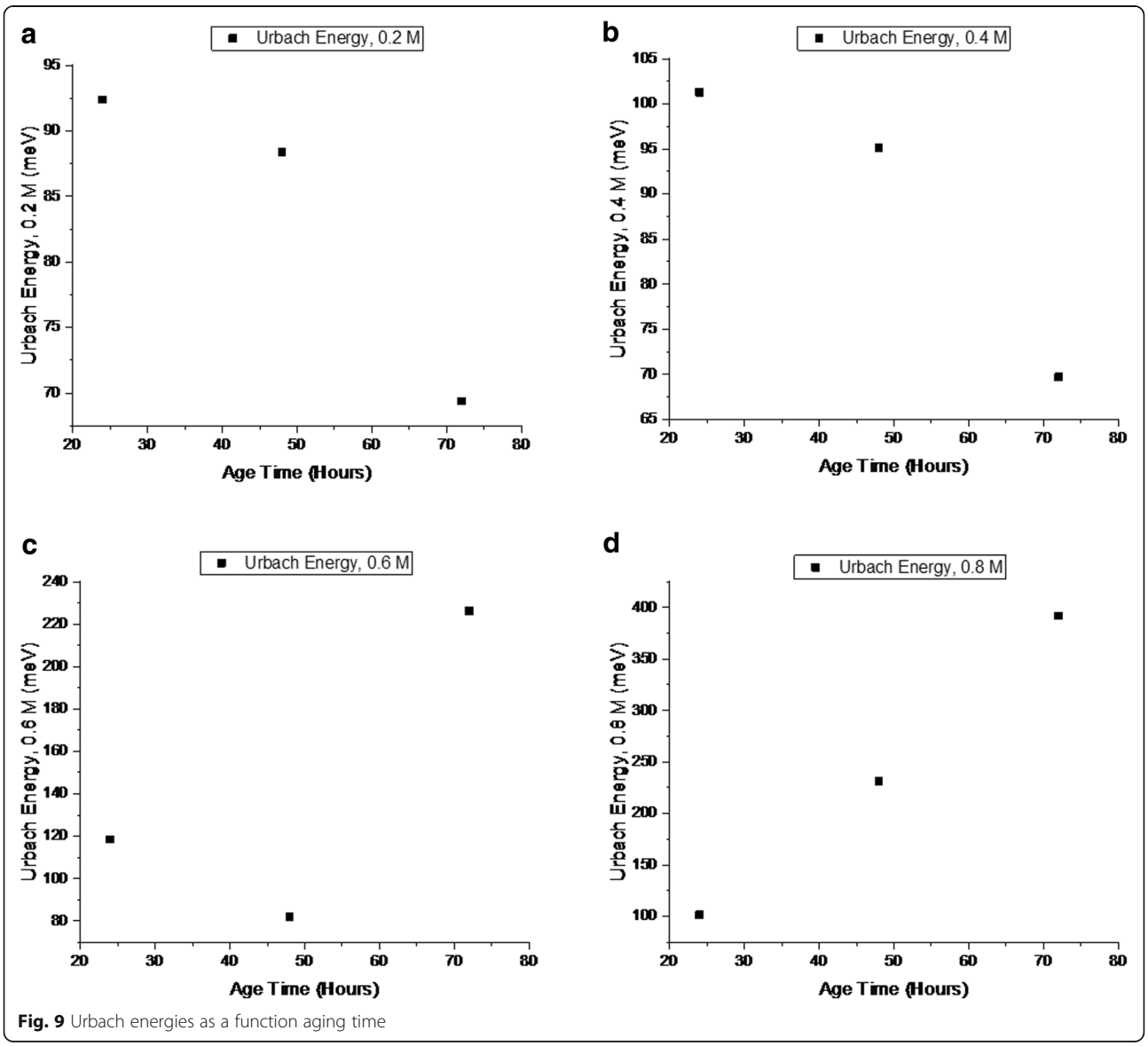

Fig. 9 Urbach energies as a function aging time

gap, E_g. Figure 5 shows the actual Tauc plots and linear extrapolations for all samples.

The band gaps are consistent with literature values. For example, Dutta et al. found band gaps of sol gel thin films from 3.27 to 3.30 eV and Bao et al. from 3.31 to 3.44 eV (Boa, Gu, & Kuang, 1998; Dutta, Mridha, & Basak, 2008). Most computed band gaps in this work are between 3.28 to 3.38 eV. The only exceptions using the Tauc method are for high concentrations at extended aging times: 0.6 and 0.8 M at 72 hours. These films have considerable scattering which results in the observed background in the Tauc plots between 2.4 and 3.2 eV being non-zero, and the linear region of the curve is less well defined. This obscures the band edge transition, making it difficult to find the linear region in the Tauc plots which is required for extrapolation. The result is that the Tauc Method is less effective for these samples. For this reason, an alternative method was used to compute the band gap in high concentration samples at extended aging times. Liu et al. use plots of dT/dλ to compare the relative positions of the band gap. The position of the peak, or where the first derivative of the dT/dλ vs wavelength curve is zero, approximates the band gap. Figure 6 shows the plots of dT/dλ for all films.

Table 2 shows the computed band gaps using both the dT/dλ method and Tauc method with the corresponding R^2 values from the linear fits. The Δ is the difference in band gap between the two methods. The difference is always small, usually close to 0.03 eV. The largest observed difference between the methods is for 0.6 M at 48 hours where the difference was 0.09 eV.

Figure 7 graphs the Band Gap as a function of aging time for each sample concentration.

Band gap is an important property, and changes in the value are representative of film quality. Shan et al. and Suchea et al. both found that a higher value for the band gap in ZnO was a result of lower-quality films which could be caused by one or more of the following: changes in crystallinity, changes in defect density, and/or changes in tensile or compressive stress (Shan, Liu, Lee, & Shin, 2007; Suchea, Christoulakis, Katharakis, Vidakis, & Koudoumas,

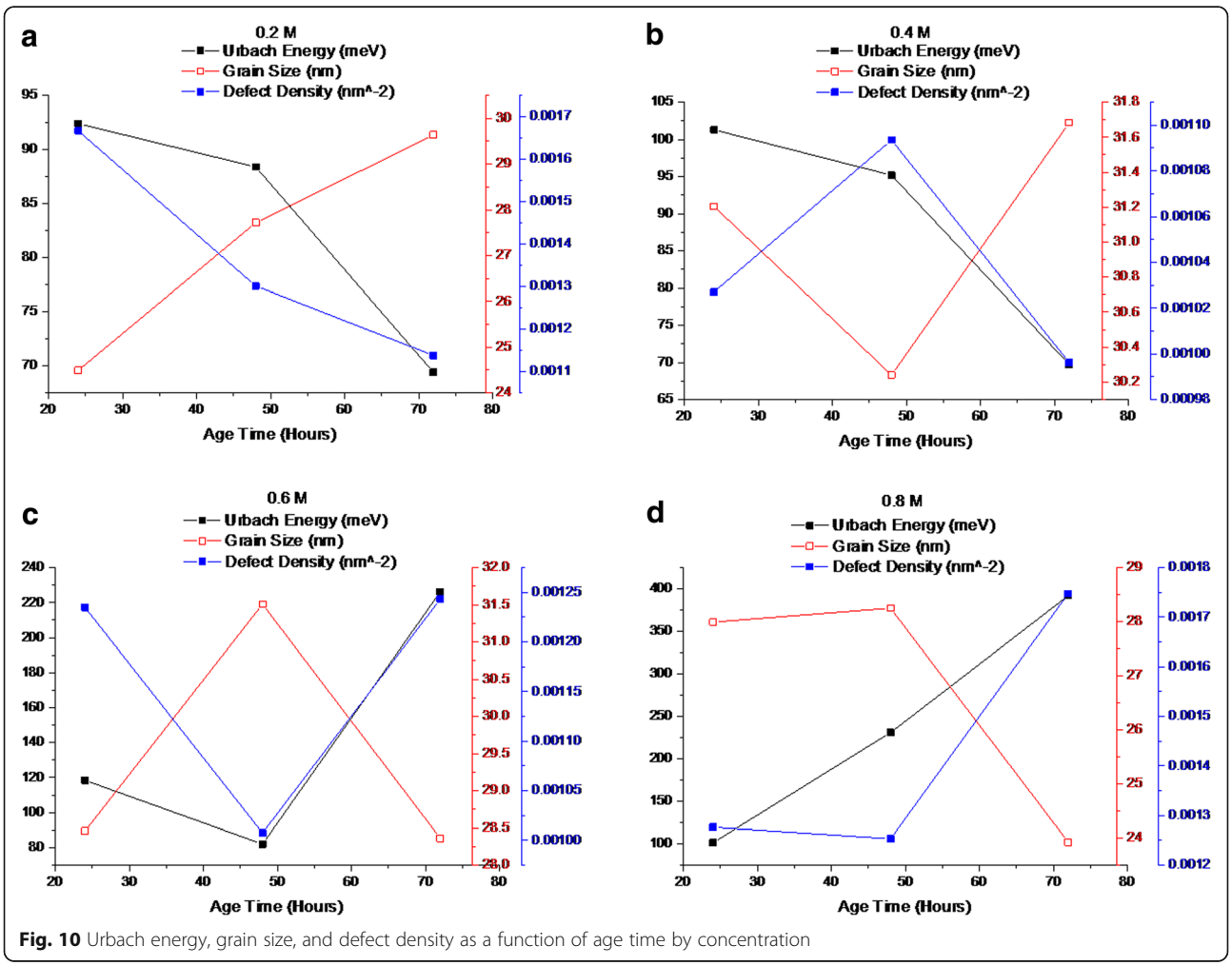

Fig. 10 Urbach energy, grain size, and defect density as a function of age time by concentration

2009). In Shan's and Suchea's work, the band gaps varied from 3.34 to 3.25 eV and 3.34 to 3.21 eV, respectively, which is similar to the range observed here of about 0.1 eV between 24 and 72 hours aging time between films of the same concentration (Shan et al., 2007; Suchea et al., 2009).

For the low concentration samples, the band gap stays constant near 3.40 eV, and there is almost no difference between 0.2 and 0.4 M samples. Only at extended aging times of 72 hours is there a noticeable decrease in the band gap for both 0.2 and 0.4 M samples. This suggests that for low concentration samples, aging must be extended for long durations, up to 72 hours, to achieve the highest quality films. The results are similar for higher concentration films only the allowable aging time decreases. Both high concentration samples display a notable decrease in their band gap after just 48 hours. This trend continues for the 0.6 M sample but remains flat for the highest concentration sample. For 0.8 M, addition aging beyond 48 does not lead to a reduction in the band gap. These results are consistent with XRD data for the grain size and crystal quality discussed above.

The band gap can be compared for each age duration as a function of concentration. This is plotted in Fig. 8.

In all cases, for the same aging time, 0.6 M results in the lowest band gap. At 24 hours, the 0.4 and 0.8 M have very similar band gaps, with the lowest concentration sample of 0.2 M having the highest band gap. By 48 hours, the accelerated aging of the higher concentration samples (discussed above) results in the 0.8 M sample having a smaller band gap than either of the lower concentrations samples (0.2 and 0.4 M). It is only after excessive aging for the 0.8 M film, at 72 hours, that the lower concentration films at 0.2 and 0.4 M show a smaller band gap. These results indicated that high concentration films near 0.6 M may, under some conditions, yield better quality films than lower concentrations films near 0.2 or 0.4 M that are more commonly cited in the literature.

Since the band gap of ZnO is defined as 3.37 eV (~368 nm), the absorption edge of ZnO is just outside of the visible region. However, as film quality decreases, band tailing increases, leading to some absorption below the fundamental band gap (Uzar, 2018). This band tailing is

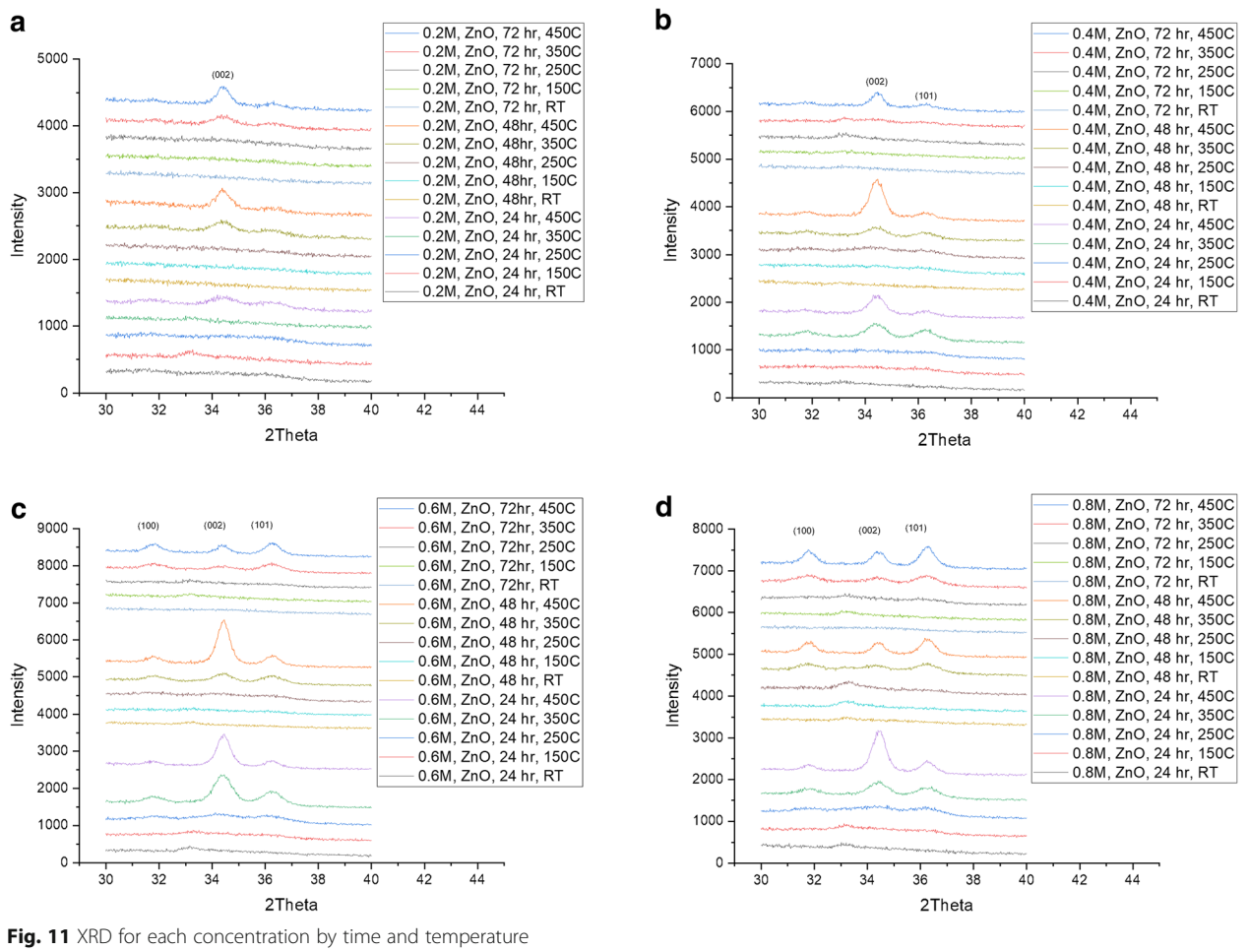

Fig. 11 XRD for each concentration by time and temperature

described by Urbach's rule (Abed, Bouzidi, Elhouichet, Gelloz, & Ferid, 2015; Dalouji et al., 2018; Tuzemen, Eker, Kavak, & Esen, 2009; Uzar, 2018):

$$\alpha = \alpha_0 + e^{\frac{h\nu}{E_u}} \tag{8}$$

where α_0 is a constant, α is the absorption coefficient, $h\nu$ is the photon energy, and E_u is the Urbach energy. The Urbach energy represents the width of the tail of localized states inside the band gap which leads to absorption below the fundamental band gap (Sandeep, Bhat, & Dharmaprakash, 2018). It is largest in materials that are amorphous and/or have a large number of defects. By plotting Ln(α) vs Ln($h\nu$) and taking the inverse of the slope, E_u can be computed (Abed et al., 2015). Figures 9 and 10 shows the computed Urbach energy as a function of aging time for each concentration.

The Urbach energies range from 70 and 100 meV for low concentration films and 80 to 400 meV for high concentration films. These values are consistent with literature for results published by Caglar et al. for similar concentrations films (Caglar, Caglar, & Ilican, 2012).

Since the Urbach energy is related to the number of defects in the film, as the defect density decreases, the Urbach Energy should also decrease. The defect density can be computed from the following equation (Bindu & Thomas, 2014; Saleem et al., 2012):

$$\delta = \frac{1}{D^2} \tag{9}$$

where δ is the defect density in nm^{-2} and the D is the grain size in nm. The following figure plots the Urbach energy (left y-axis) compared to the grain size and defect density (right 2 axes) (Fig. 10).

In general, there is good agreement found between the Urbach energy and the grain size (or defect density). As the grain size increases, the Urbach energy decreases. Thus, determining the condition necessary for the largest grain size is equivalent to minimizing the defects that contribute to band tailing. This improvement in the

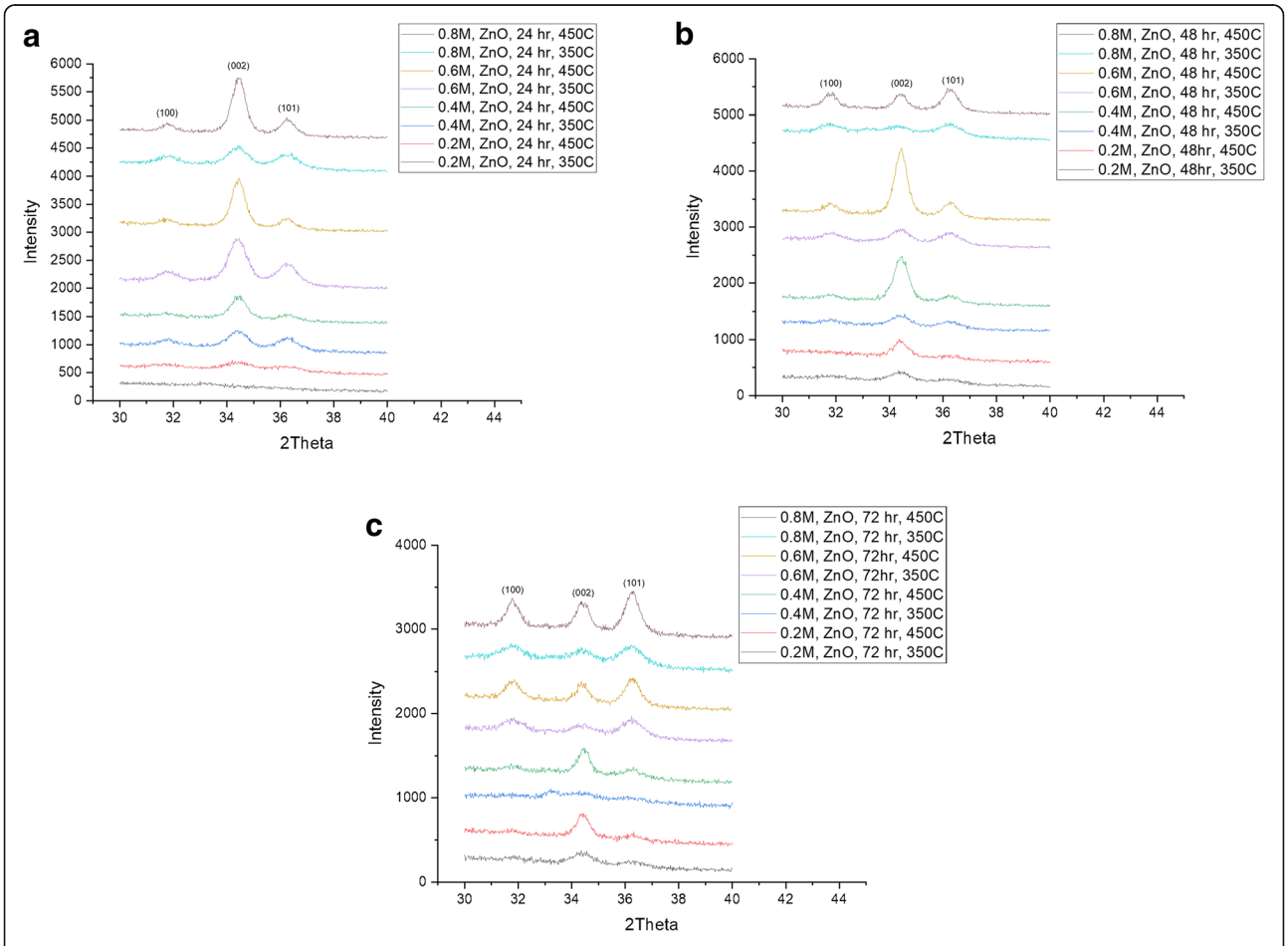

Fig. 12 XRD of high-temperature annealed films by age time

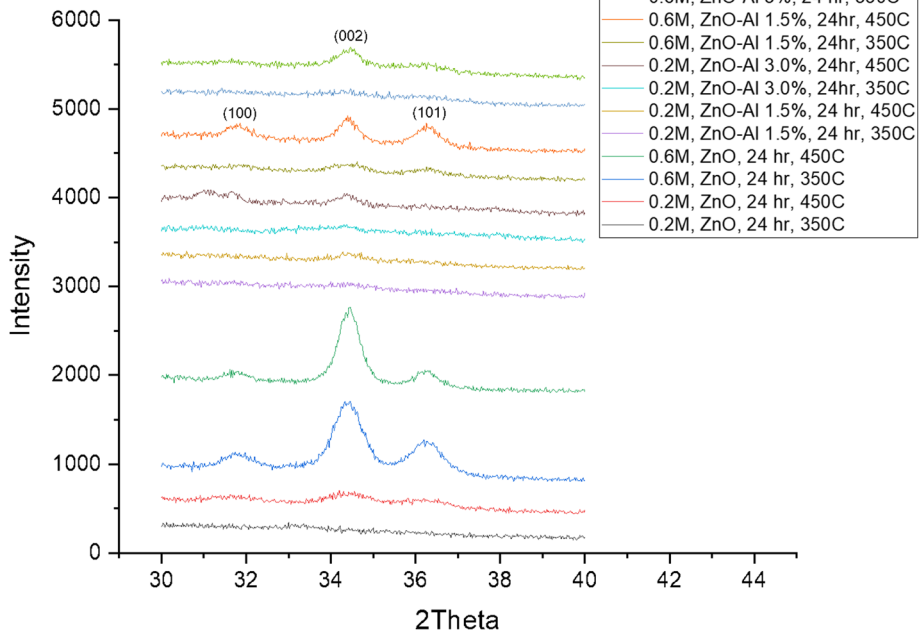

Fig. 13 XRD of Al-doped ZnO (1.5 and 3% Al) compared to undoped ZnO

crystal structure results in an improvement in the optical properties (a reduction in band tailing).

Next the impact of annealing and doping on the structure of the thin films is investigated. All samples were annealed from 150 to 450 °C in 100 °C increments for 1 hour. Peak position and intensities are compared. Aluminum was used to an n-type dopant with concentrations of 1.5 and 3%, in low concentration Zn precursor films (0.2 M) and high concentration Zn precursor (0.6 M), with the same annealing series. Figure 11 shows the data for the undoped thin films.

Figure 11 displays the transition from weak, or no, diffraction peaks to strong diffraction peak intensity as temperature increases. For all films, the diffraction peaks are very weak for RT, 150 °C and 250 °C annealed samples. Starting at 350 °C and continuing to 450 °C, stronger diffraction peaks are observed in most films. And as concentration increases, additional diffraction peaks become more likely at elevated temperatures. At 0.2 M concentration, only the (002) is observed, while in the 0.4 M samples, a weak (101) is present in some films. The high concentration films display three diffraction peaks from the (100), (002), and (101) in some of the films. In most cases, 350 °C is the minimum temperature, at 1-hour annealing, for diffraction peaks to be present. Figure 12 displays the high-temperature (350 and 450 °C) annealing data.

For low concentration films, all diffraction peaks are weak for an age time of 24 hours. Higher concentration films display a visible (002) at 24 hours of aging. Figure 12 shows that, in general, higher concentration films tend to have stronger diffraction peaks intensity at each set of comparable conditions (temperature and age time). In particular, the 0.6-M film at 24 hours displays a very large diffraction peak even at 350°C. One advantage of higher concentration films would be lower required annealing conditions, in addition to the reduced age time discussed above.

Figure 13 shows the diffraction data for Al-doped ZnO thin films and their undoped ZnO references.

When Al is added to ZnO, there are two common incorporation methods (Flickyngerova et al., 2008; Ting & Tsai, 2001). Al can be a substitute for Zn atoms in the lattice and thereby become an n-type dopant adding free electrons to the conduction band. Al can also be incorporated as an interstitial defect within the lattice. The former is preferred, and the latter is not. If Al substitutes

Table 3 (002) peak position for doped and undoped ZnO

Concentration (M)	Age time (Hours)	Annealing temp (°C)	Al percent	(002) Peak position, 2Theta
0.6	24	450	0	34.46
0.6	24	450	1.5	34.40
0.6	24	450	3.0	34.46

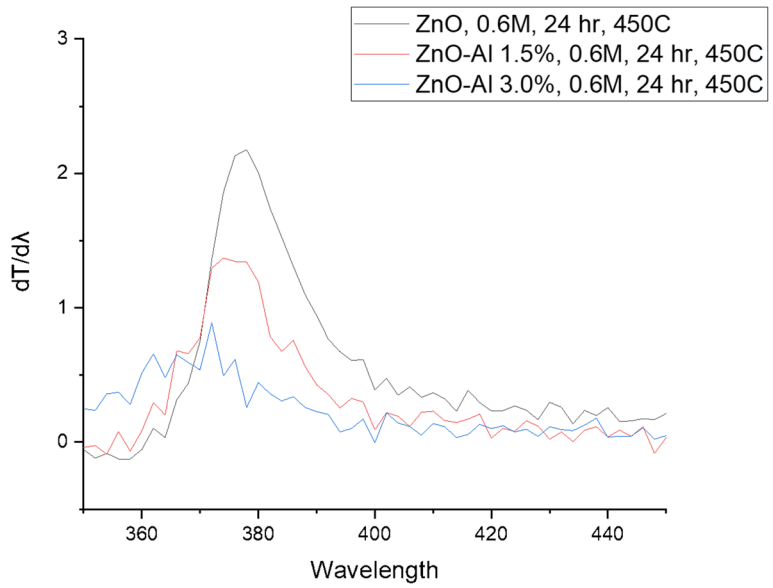

Fig. 14 dT/dλ plots for ZnO and ZnO-Al

for Zn, it will reduce the lattice parameter and thus shift the diffraction peaks to higher 2Theta values, while Al as an interstitial defect shifts the diffraction peaks to lower 2Theta values. This is commonly understood in terms of Vegard's law, since the ionic radius of aluminum is 0.53 Å and that of Zinc is 0.60 Å (Nakrela et al., 2016). The 0.2-M-thin films do not display diffraction peaks with either 1.5 or 3.0% Al, suggesting that higher temperatures or longer annealing is required. The higher concentration films do show a (002) diffraction peak for 450 °C annealing for 1 hour. This result is consistent with the data discussed for the undoped ZnO, namely, that for shorter annealing durations, higher concentration films display higher crystallinity than lower concentration films, and it is thus easier for Al to substantially replace Zn in the lattice since 0.6 M is more crystalline.

Since there are two competing factors (substitutional and interstitial Zn incorporation) that shift the diffraction peak in opposite directions, the relationship between the 2Theta shift and the Al doping is often complicated. For example, Nakrela et al. recently found that 2% Al doping decreased the lattice spacing, while 4% Al doping increased the lattice space (Nakrela et al., 2016). This was explained by 2% Al being predominately substitutional and the 4% Al samples being predominately interstitial. Table 3 suggests that a significant fraction of the Al is interstitial at 1.5%. At 3.0% more Al is substitutional, leading to a larger 2Theta value and a smaller lattice constant.

Figure 14 displays the optical data for ZnO-Al and the ZnO reference film.

ZnO-Al is known to have higher band gap than undoped ZnO, and this results in the blue shift observed in Fig. 14 (You et al., 2015). Figures 13 and 14 provide evidence that Al-doped ZnO can be fabricated via this method, but additional annealing beyond 450°C for 1 hour is required before the films become highly crystalline.

Conclusion

ZnO thin films were deposited on glass substrates using sol gel. Both the concentration and aging time were investigated. The optical and structural properties were studied using absorption and XRD. The largest grain sizes were found in films with concentration of 0.4 and 0.6 M. Higher concentration films were also found to age more quickly, reaching peak quality sooner than lower concentration films. Lower concentrations required 72 hours to achieve the largest grain size and smallest band gap, while higher concentration samples required just 48 hours. The % transmittance tended to decrease with increasing aging time for all samples. Lower concentration samples displayed both higher % transmittance and a smaller fall off with aging time.

Supplementary information

Supplementary information accompanies this paper at https://doi.org/10.1186/s40712-019-0113-6.

Additional file 1. XRD Data by Concentration and Aging Time.

Acknowledgements

I wish to acknowledge Oregon State University and ATAMI (Advance Technology and Manufacturing Institute) for their support in the commercialization of clean energy technologies.

Authors' contributions

The author read and approved the final manuscript.

Funding
I have no funding sources to declare.

Availability of data and materials
All data is made available within the text of the document or the attached Additional file 1.

Ethics approval and consent to participate
Not applicable.

Consent for publication
Not applicable.

Competing interests
The author declares that he has no competing interests.

Received: 19 August 2019 Accepted: 15 November 2019
Published online: 29 January 2020

References

Abed, C., Bouzidi, C., Elhouichet, H., Gelloz, B., & Ferid, M. (2015). Mg doping induced high structural quality of sol-gel ZnO nanocrystals: application in photocatalysis. *Applied Surface Science, 349*, 855–863.

Amari, R., Mahroug, A., Boukhari, A., Deghfel, B., & Selmi, N. (2018). Structural, optical and luminescence properties of ZnO thin films prepared by sol-gel spin-coating method: effect of precursor concentration. *Chinese Physics Letter., 35*(1), 016801.

Bindu, P., & Thomas, S. (2014). *Journal of Theoretical and Applied Physics., 8*, 123–134. https://doi.org/10.1007/s40094-014-0141-9.

Boa, D., Gu, H., & Kuang, A. (1998). Sol-gel derived c-axis orientated ZnO thin films. *Thin Solid Films, 312*, 37–39.

Caglar, Y., Caglar, M., & Ilican, S. (2012). Microstructural, optical and electrical studies on sol gel derived ZnO and ZnO:Al films. *Current Applied Physics, 12*, 963–968.

Chu, M. C., You, H. C., Meena, J., Shieh, S. H., Shao, C. Y., Chang, F. C., & Ko, F. H. (2012). Facile electroless deposition of zinc oxide ultrathin film for zinc acetate solution-processed transistors. *Internationl Journal of Electrochemical Science., 7*, 5977–5989.

Dalouji, V., Solaymani, S., Dejam, L., Elahi, S. M., Rezaee, S., & Mehrparvar, D. (2018). *Chinese Physics Letter, 35*(*2*), 027701.

Demichelis, F., Minetti-Mezzetti, E., Smurro, V., Tagliagerro, A., & Tresso, E. (1985). Physical properties of chemical sprayed tin oxide and indium tin oxide transparent conductive films. *Journal Physics D: Applied Physics, 18*, 1825–1832.

Dutta, M., Mridha, S., & Basak, D. (2008). Effect of sol concentration on the properties of ZnO thin films prepared by sol-gel technique. *Applied Surface Science., 254*, 2743–2747.

El Hamidi, A., Meziane, K., El Hichou, A., Jannane, T., Liba, A., El Haskouri, J., Amoros, P., & Almaggoussi, A. (2018). Refractive index controlled by film morphology and free carrier density in undoped in ZnO through sol-pH variation. *Optik, 158*, 1139–1146.

Flickyngerova, S., Khtereva, K., Stenova, V., Hasko, D., Novotny, I., Tvarozek, V., Sutta, P., & Vavrinsky, E. (2008). Structural and optical properties of sputtered ZnO thin films. *Applied Surface Science, 254*, 3643–3647.

Goncalves, R. S., Barrozo, P., Brito, G. I., Viana, B. C., & Cunha, F. (2018). The effect of thickness on optical, structural and growth mechanism of ZnO thin films prepared by magnetron sputtering. *Thin Solid Films, 661*, 40–45.

Gueymard, C.A., Myers, D., Emery, K. Proposed reference irradiation spectra for solar energy systems testing. Solar Energy. Vol 73. No. 6. Pg 443-467. (2002)

Ibrahim, N. B., Al-Shomar, S. M., & Ahmed, S. H. (2013). Effect of aging time on the optical, structural and photoluminescence properties of nanocrystalline ZnO films prepared by a sol-gel method. *Applied Surface Science, 283*, 599–602.

Janardhanam, V., Jyothi, I., Lee, S. N., Reddy, V. R., & Choi, C. J. (2019). Rectifying and breakdown voltage enhancement of Au/n-GaN Schottky diode with Al-doped ZnO films and its structural characterization. *Thin Solid Films., 676*, 125–132.

Janotti, A., & Van de Walle, C. (2009a). Fundamentals of zinc oxide as a semiconductor. *Reports on Progress in Physics., 72*, 126501 (29 pp).

Janotti, A., & Van de Walle, C. G. (2009b). Fundamentals of zinc oxide as a semiconductor. *Reports on Progress in Physics., 72*, 126501.

Jayaraman, V. K., Alvarez, A. M., Bizarro, M., & Amador, M. (2018). Effect of acetic acid and water content in the spray solution on structural, morphological, optical and electrical properties of Al and in co-doped zinc oxide thin films. *Journal of Materials Science: Materilas in Electronics, 29*, 15321–15328.

Mayer, M. A., Yu, K. M., Speaks, D. T., Denlinger, J. D., Reichertz, L. A., Beeman, J. W., Haller, E. E., & Walukiewicz, W. (2012). Band gap engineering of oxide photoelectrodes: characterization of $ZnO_{1-x}Se_x$. *The Journal of Physical Chemistry. C, 116*, 15281–15289.

Meng, X., Zhao, C., Xu, B., Wang, P., & Liu, J. (2018). Effects of the annealing temperature on the structure and up-conversion photoluminescence of ZnO film. *Journal of Materials Science & Technology, 34*, 2392–2397.

Nakrela, A., Benramdane, N., Bouzidi, A., Kebbab, Z., Medles, M., & Mathieu, C. S. (2016). Site location of Al-dopant in ZnO lattice by exploiting the structural and optical characterisation of ZnO:Al thin films. *Results in Physics*, 6, 133–138..

Rabina, B., Rai, S., & Swain, B. P. (2019). Spectroscopic characterization of CVD grown zinc oxide nanowires. *Materials Science in Semiconductor Processing, 102*, 104592.

Rajeh, S., Khirouni, K., Amlouk, M., & Guermazi, S. (2015). Experiments on ZnO:Ni thin films with under 1% nickel content. *Optics & Laser Technology., 69*, 113–121.

Saleem, M., Fang, L., Ruan, H. B., Wu, F., Huang, Q. L., Xu, C. L., & Kong, C. Y. (2012). Effect of zinc acetate concentration on the structural and optical properties of ZnO thin films deposited by sol-gel method. *International Journal of Physical Science., 7*(23), 2971–2979.

Sandeep, K. M., Bhat, S., & Dharmaprakash, S. M. (2018). Role of defect states on nonlinear properties of 8 MeV electrons irradiated zinc oxide thin films under off-resonant regime. *Ceramics International., 44*, 9063–9069.

Shan, F. K., Liu, G. X., Lee, W. J., & Shin, B. C. (2007). The role of oxygen vacancies in epitaxial-deposited ZnO thin films. *Journal of Applied Physics., 101*, 053106.

Suchea, M., Christoulakis, S., Katharakis, M., Vidakis, N., & Koudoumas, E. (2009). Influence of thickness and growth temperature on the optical and electrical properties of ZnO thin films. *Thin Solid Films, 517*, 4303–4306.

Tan, S. T., Chen, B. J., Sun, X. W., Fan, W. J., Kwok, H. S., Zhang, X. H., & Chua, S. J. (2005). Blue shift of optical band gap in ZnO thin films grown by metal-organic chemical-vapor deposition. *Journal of Applied Physics., 98*, 013505.

Tauc, J., Grigorovici, R., & Vancu, A. (1966). Optical properties and electronic structure of amorphous germanium. *Physica Status Solidi., 15*(2), 627.

Terasako, T., Ochi, Y., Yagi, M., Nomoto, J., & Yamamoto, T. (2018). Structural and optical properties of ZnO films grown on ion-plated Ga doped ZnO buffer layers by atmospheric-pressure chemical vapor deposition using Zn and H_2O as source materials. *Thin Solid Films, 663*, 79–84.

Ting, J. M., & Tsai, B. S. (2001). DC reactive sputter deposition of ZnO:Al thin film on glass. *Materials Chemistry and Physics, 72*, 273–277.

Tuzemen, E. S., Eker, S., Kavak, H., & Esen, R. (2009). *Applied Surface Science., 255*, 6195–6200.

Uzar, N. (2018). Investigation of detailed physical properties and solar cell performances of various type rare earth elements doped ZnO thin films. *Journal of Materials Science: Materials in Electronics, 29*, 10471–10479.

Wang, J., Wang, Z., Huang, B., Ma, Y., Liu, Y., Qin, X., Zhang, X., & Dia, Y. (2012). Oxygen vacancy induced band-gap narrowing and enhanced visible light photocatalytic activity of ZnO. *ACS Applied Materials & Interfaces., 4*, 4024–4030.

Wannes, H. B., & Zaghousani, R. B. (2018). Study of the stabilizer influence on the structural and optical properties of sol gel spin coated zinc oxide films. *Materials Science in Semiconductor Processing, 74*, 80–87.

Yan, X. Y., Yao, C. B., Li, J., Hu, J. Y., Li, Q. H., & Yang, S. B. (2016). Structural, photoluminescence and picosecond nonlinear optical effects of in-doped ZnO nanowires. *Optical Materials, 55*, 73–77.

Yaun, H., Xu, M., & Huang, Q. Z. (2014). Effects of pH of the precursor sol on structural and optical properties of Cu-doped ZnO thin films. *Journal of Alloys and Compound, 616*, 401–407.

You, Q., Cai, H., Hu, Z., Liang, P., Prucnal, S., Zhou, S., Sun, J., Xu, N., & Wu, J. (2015). Blue Shift in absorption edge and widening of band gap of ZnO by Al doping and Al-N co-doping. *Journal of Alloys and Compounds., 644*, 528–533.

Yu, J., Zhang, M., Zhang, Z., Wang, S., & Wu, Y. (2019). Hybrid-functional calculations of electronic structure and phase stability of MO (M = Zn, Cd, Be, Mg, Ca, Sr, Ba) and related ternary alloy $M_xZn_{1-x}O$. *RSC Advances, 9*, 8507.

Zen, H., Duan, G., Li, Y., Yang, S., Xu, X., & Cai, W. (2010). Blue luminescence of ZnO nanoparticles based on non-equilibrium processes: defect origins and emission controls. *Advanced Functional Materials., 20*, 561–572.

Znaidi, L. (2010). Sol-gel-deposited ZnO thin films: a review. *Materials Science and Engineering B., 174*, 18–30.

Publisher's Note